Direct Analytical Solution for the Electric Field Distribution at the Conductor Surfaces of Coplanar Waveguides

Matthew Gillick, *Student Member, IEEE,* Ian D. Robertson, *Member, IEEE,* and Jai S. Joshi, *Senior Member, IEEE*

Abstract— **A new analytical method of evaluating the electric field distribution across the conductor surfaces of coplanar waveguides (CPW's) is presented. Here, a series of conformal mappings are employed to transform the CPW's geometry and field distribution into a uniform image domain, to facilitate a direct field solution. The cumulative electric flux distribution across each conductor surface within the dielectric substrate is studied, and its effects on coupling and propagation modes are described. Direct solutions for the quasistatic normal electric field components are presented together with their graphical representations. Numerical computations show how the total electric flux terminating on the CPW's conductor surfaces varies in terms of the CPW's geometry and substrate parameters.**

I. Introduction

With the growing interest in Coplanar Waveguides (CPW's) for the design of hybrid and monolithic microwave integrated circuits (MMIC's), the need for accurate analytical modeling of the structure has increased. However, unlike microstrip circuits, there exists a relatively limited amount of theoretical analysis of this CPW transmission line. The principal advantage of CPW, over microstrip, as an integrated transmission line is the simplification of the circuit fabrication process due to the ground plane being on the same substrate surface as the signal line. This improved design feature offers reduced parasitic inductances to ground when devices such as FET's or HEMT's are employed. Furthermore, it is possible to fabricate MMIC's without the need for via holes. Such circuit designs incorporating CPW's require an extensive study of their field distributions in order to characterize their field confinements and coupling effects. Practical realizations of CPW's usually have an additional ground conducting plane beneath the substrate. The main advantages of this back face metallization are principally to reduce radiation effects, to raise the effective permittivity of the transmission line and to improve heat dissipation. The standard CPW plus this additional conducting ground plane is often called grounded CPW.

A number of theoretical analyses of CPW's has been reported [1]–[12]. The mapping function, first presented by Wen [2], employed a zeroth-order quasistatic approximation, to estimate the phase velocity and characteristic impedances of CPW lines, where the method was later extended for the design of a CPW directional coupler [3]. From a modification of Wen's earlier method, Ghione and Naldi [4]–[5] produced parameters for both grounded and ungrounded CPW's using intermediate mappings, and later on, extended the analysis to take into account parasitic effects [6]. Various approaches were employed to analyze CPW configurations based on the quasistatic approximation, including the relaxation method [7], and the conformal mapping method [8]. In determining the spatial waveforms of the electric field for CPW's, Liang *et al.* [9] used the time-domain finite-difference method for their wave-analysis. The electrostatic field of two semi-infinite electrodes placed on top of a layered dielectric medium was modeled extensively by Marcuse [10], using the point matching method and, recently, Chang *et al.* [11] used a variational conformal mapping technique for plotting the field distributions for CPW's.

Many of the recent field mapping techniques, like the finite-difference method, require relatively lengthy computation time involving many successive iterations. The spectral-domain technique, which has previously been used to analyze CPW's [12], also requires extensive numerical evaluation. In this paper, a direct computational method of electric field synthesis, in terms of complete and incomplete elliptic integrals, is presented, that involves conformal mapping techniques. More specifically, we extend the conformal transformation approach to analyse the field distribution of the quasi-TEM mode for CPW's. While it is true that the quasistatic analysis is only rigourously valid at zero frequency, the range of use of the quasi-TEM approximation is predicted to extend well beyond 20 GHz, for a substrate thickness of 0.3 mm [6]. Therefore, the following frequency-independent analysis applies only to the transverse electric field, since the magnitude of the longitudinal electric field component is less than 1% of the transverse field [11]. The mapping techniques employed here transform the original infinite domain into a finite image domain. This mapping is able to represent the field singularities near the CPW's conductor edges. The normal electric field over all

Manuscript received January 3, 1992; revised April 14, 1992. This work was supported by the Science and Engineering Research Council (SERC) UK and by British Aerospace Space Systems Limited, UK.

M. Gillick and I. D. Robertson are with the Communications Research Group, Department of Electronic and Electrical Engineering, King's College, University of London, Strand, London, UK, WC2R 2LS.

J. S. Joshi is with Satellite Payload Engineering Department, British Aerospace Space Systems Limited, Argyle Way, Stevenage, Herts, UK, SG1 2AS.

IEEE Log Number 9204020.

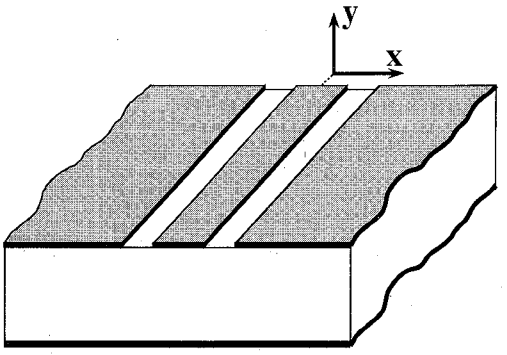

Fig. 1. Grounded coplanar waveguide structure.

the CPW's conductor surfaces, together with their cumulative electric flux distributions, are examined.

II. Method of Analysis for Electric Field Modeling

The coplanar waveguide configuration under analysis is shown in Fig. 1, where the ground planes are assumed to be sufficiently wide as to be considered infinite in the analytical model. All metallic conductors are assumed to be infinitely thin and perfectly conducting. The corresponding electric field distribution is shown in Fig. 2(a), where the central conductor, of width $2a$, is placed between the two upper ground planes, of spacing $2b$, which are located on a substrate of thickness h, with relative permittivity ϵ_r. When considering grounded CPW's it is assumed that the air-dielectric boundary between the center conductor and the upper ground plane behaves like a perfect magnetic surface. This ensures that no electric field lines emanating into the air from the center conductor cross the air-dielectric boundary. Transverse symmetry is assumed so that no antisymmetric mode is excited. In so far as the electric field is concerned, it is sufficient to consider only the right half plane of the guiding structure, where a perfect magnetic surface exists at $x = 0$. First, consider the E-field within the substrate of this right half plane as shown in Fig. 2(b). A sequence of two conformal transformations may be employed to evaluate the capacitance per unit length of this section [2], as shown in Fig. 2(c) and (d). The resultant electric field lines may be considered as a set of equally spaced lines orthogonal to the parallel plates of this capacitor in the finite image z_1 domain, as shown in Fig. 2(d). By inverse mapping of these lines, from the z_1 domain back to the original z domain, we may construct the electric field distribution on all the conductor surfaces of the grounded CPW. Therefore, it can be said that the density of lines is a relative indication of the electric field strength for a given homogeneous, isotropic medium. Looking at the first conformal mapping, the field between the semi-infinite strips will be mapped to the lower half of the t plane, using the Schwartz–Christoffel transformation:

$$t = \cosh^2\left(\frac{\pi z}{2h}\right) \qquad z = x + iy$$

$$\text{where } t_2 = \cosh^2\left(\frac{\pi a}{2h}\right) \quad \text{and} \quad t_3 = \cosh^2\left(\frac{\pi b}{2h}\right). \tag{1}$$

For the second conformal mapping, the E-field within the

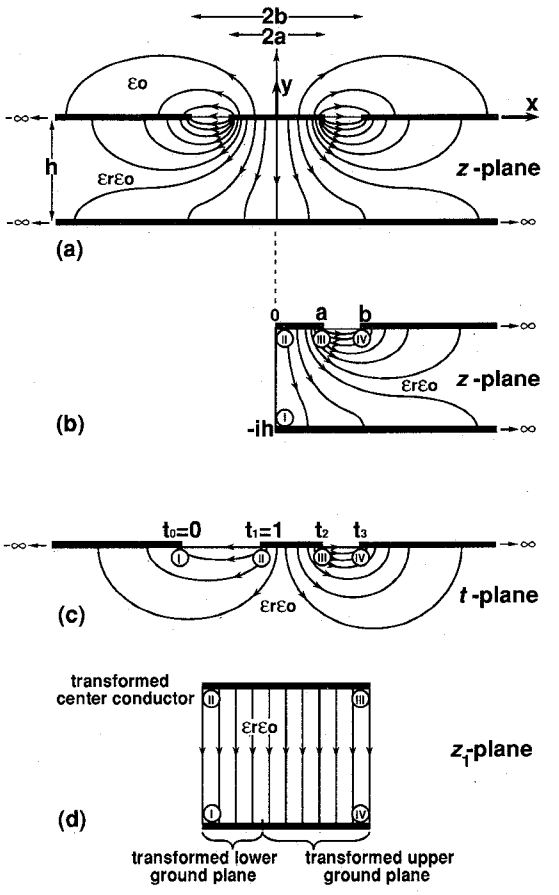

Fig. 2. Spatial distribution for the transverse components of the electric field, (a) for the complete structure in the z domain, (b) for one half of the structure within the dielectric substrate in the z domain, (c) for the first transformation in the t domain, and (d) for the final transformation in the z_1 domain.

lower half of the t plane is transformed to the image z_1 domain using:

$$z_1 = \int_0^t \frac{dt}{\sqrt{t(t-t_3)(t-t_2)(t-1)}}. \tag{2}$$

For the finite z_1 domain, the electric field is uniform, i.e. $E_y(z_1)$ is a constant. The transvere electric field lines terminating on the surface of a perfect conductor must be perpendicular to that surface. As a result, there only exists an E_y component over the conductor surfaces of the CPW for the TE field. Thus, from (2), the resultant normal electric field distribution within the substrate is thus obtained using the following conformal mapping:

$$E_y(z)_{\text{sub}} \propto \frac{dz_1}{dz}$$
$$= 2\left\{\left[\cosh^2\left(\frac{\pi z}{2h}\right) - \cosh^2\left(\frac{\pi a}{2h}\right)\right]\right.$$
$$\left.\left[\cosh^2\left(\frac{\pi z}{2h}\right) - \cosh^2\left(\frac{\pi b}{2h}\right)\right]\right\}^{-1/2} \tag{3}$$

Of the total electric field, the fraction within the substrate [2]

maybe expressed as

$$A_1 = \frac{\dfrac{K(k_1)}{K(k_1')}}{\dfrac{K(k)}{K(k')} + \dfrac{K(k_1)}{K(k_1')}} \tag{4}$$

where

$$k_1 = \frac{\tanh\left(\dfrac{\pi a}{2h}\right)}{\tanh\left(\dfrac{\pi b}{2h}\right)} \tag{5}$$

and where the modulus is $k = a/b$. $K(k)$ is the complete elliptical integral of the first kind, and $k' = (1-k^2)^{1/2}$ is the complementary modulus. For the air filled upper half plane of Fig. 2(a), we have the electric field distribution immediately over the upper conductors as

$$E_y(z)_{\text{air}} = \frac{\dfrac{K(k)}{K(k')}}{\sqrt{[x^2-a^2][x^2-b^2]}} \qquad \text{for } x < a \text{ or } x > b. \tag{6}$$

Similarly, (3) leads to the following expressions for the TE field distribution across the conductor surfaces within the substrate, as is shown in (7a) at the bottom of the page, when $z = x + i0$. and (7b), which is also at the bottom of the page, when $z = x - ih$. For the sake of brevity, only the electric fields within the substrate will be computed here. Fig. 3 shows the normalized normal electric field distributions $E_y/E_{y\,\min}$ over all the conductor surfaces within the substrate, evaluated from (7), for several values of k and h (ie, $E_{y\,\min}$ is set to unity at $x = 0$) for graphs 3a, 3b and 3c. The electric field strengths at the center and upper ground conductors, as depicted in Fig. 3(a) and (b), decay more rapidly as k approaches unity. In Fig. 3(c) the fields are shown to exhibit edge singularities at the conductor edges. In practice, this gives a maximum electric field intensity over the conductor edges for CPW's, as expected. Fig. 3(d) shows the variation in electric field strength at the lower ground plane as k and h vary. These field variations are described by (7b). This graph is normalized in the sense that the electric flux emanating from the center conductor into the substrate remains constant, as described in the following section. As expected, the electric field strength intensifies in the region beneath the center conductor at $y = -h$ as the substrate thickness decreases.

III. Analytic Formulas for the Cumulative Flux Distribution

Quantifying the field intensity at the conductor edges is of great importance when determining parameters such as the insertion loss for a given structure. The previous section investigated the variation of the electric field strength E_y at the conductor surfaces. The following formulas describe how the total normal electric field for grounded CPW's is divided up, and also calculates what fraction of electric flux terminates at each conductor. The analytic formulas of these distributions for all the conductor surfaces can be determined as follows.

A. Upper Ground Plane

The integral of the electric flux distribution per unit length on the upper ground plane within the substrate is given by

$$\int_{z=b+i0}^{z=x+i0} \epsilon_0 \epsilon_r E_y dx \propto \int_{t_3}^{t} \frac{dt}{\sqrt{t(t-t_3)(t-t_2)(t-1)}} = gF(\varphi_1, k_1) \qquad \text{for } t_3 < t < \infty \tag{8}$$

where

$$g = 2\left[\sinh\left(\frac{\pi b}{2h}\right)\cosh\left(\frac{\pi a}{2h}\right)\right]^{-1} \tag{9}$$

and

$$\varphi_1 = \arcsin\sqrt{\frac{t_2(t-t_3)}{t_3(t-t_2)}} = \arcsin\left[\frac{\cosh\left(\dfrac{\pi a}{2h}\right)}{\cosh\left(\dfrac{\pi b}{2h}\right)}\sqrt{\frac{\cosh^2\left(\dfrac{\pi x}{2h}\right)-\cosh^2\left(\dfrac{\pi b}{2h}\right)}{\cosh^2\left(\dfrac{\pi x}{2h}\right)-\cosh^2\left(\dfrac{\pi a}{2h}\right)}}\right] \tag{10}$$

and where $F(\varphi_1, k_1)$ is the incomplete elliptic integral of the first kind, written in Jacobi's notation. Of the total electric flux emanating from the center conductor, the fraction within the substrate maybe expressed as

$$A_2 = \frac{\epsilon_r \dfrac{K(k_1)}{K(k_1')}}{\dfrac{K(k)}{K(k')} + \epsilon_r \dfrac{K(k_1)}{K(k_1')}} \tag{11}$$

$$E_y(z)_{\text{sub}} = \frac{2\dfrac{K(k_1)}{K(k_1')}}{\sqrt{\left[\cosh^2\left(\dfrac{\pi x}{2h}\right)-\cosh^2\left(\dfrac{\pi a}{2h}\right)\right]\left[\cosh^2\left(\dfrac{\pi x}{2h}\right)-\cosh^2\left(\dfrac{\pi b}{2h}\right)\right]}} \tag{7a}$$

$$E_y(z)_{\text{sub}} = \frac{2\dfrac{K(k_1)}{K(k_1')}}{\sqrt{\left[\sinh^2\left(\dfrac{\pi x}{2h}\right)+\cosh^2\left(\dfrac{\pi a}{2h}\right)\right]\left[\sinh^2\left(\dfrac{\pi x}{2h}\right)+\cosh^2\left(\dfrac{\pi b}{2h}\right)\right]}} \tag{7b}$$

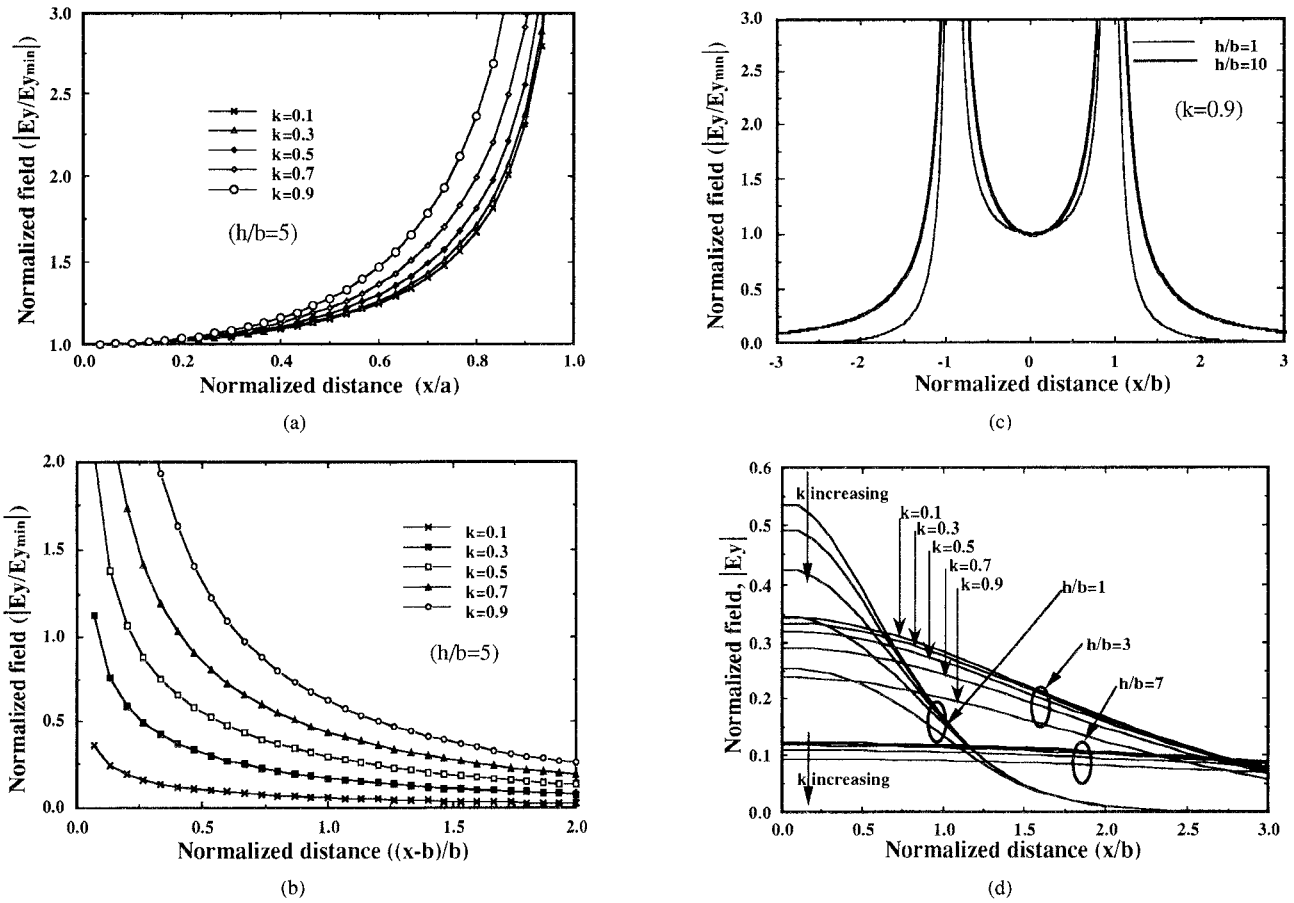

Fig. 3. Normalized field distributions over the conductor surfaces within the substrate, as a function of k and h, (a) for the center conductor, (b) for the upper ground plane, (c) for the complete center conductor and upper ground planes, and (d) for the lower ground plane.

Equation (8) can thus be expressed as

$$\int_{z=b+\imath 0}^{z=x+\imath 0} \epsilon_0 \epsilon_r E_y dx = A_2 \frac{F(\varphi_1, k_1)}{K(k_1)} \qquad \text{for } t_3 < t < \infty. \tag{12}$$

The total electric field flux terminating on the upper ground plane within the substrate may be expressed as

$$\int_{z=b+i0}^{z=\infty+\imath 0} \epsilon_0 \epsilon_r E_y dx = A_2 \frac{F\left(\arcsin\left[\dfrac{\cosh\left(\frac{\pi a}{2h}\right)}{\cosh\left(\frac{\pi b}{2h}\right)}\right], k_1\right)}{K(k_1)}. \tag{13}$$

Shown in Fig. 4, is the cumulative flux distributions beneath the upper ground plane as a function of the CPW's geometry. The plots in Fig. 4(a), based on (8), show what fraction of the total electric flux terminates on this upper ground plane within a given distance from the upper ground plane edge, (ie, 70% of A_2 terminates in the region $1 < x/b < 2$ with $h/b = 10$ and $k = 0.9$, whereas only 4% of A_2 terminates in the same region when $h/b = 1$ and $k = 0.1$).

B. Lower Ground Plane

The integral of the electric flux distribution on the lower ground plane is given by

$$\int_{z=-\imath h}^{z=x-\imath h} \epsilon_0 \epsilon_r E_y dx \propto \int_t^0 \frac{dt}{\sqrt{t(t-t_3)(t-t_2)(t-1)}}$$

$$= gF(\varphi_2 . k_1) \qquad \text{for } -\infty < t < 0 \tag{14}$$

$$\varphi_2 = \arcsin\sqrt{\frac{t(t_3-1)}{t_3(t-1)}} = \arcsin\left[\tanh\left(\frac{\pi b}{2h}\right)\tanh\left(\frac{\pi x}{2h}\right)\right]. \tag{15}$$

Equation (14) can thus be expressed as

$$\int_{z=-ih}^{z=x-ih} \epsilon_0 \epsilon_r E_y dx = A_2 \frac{F(\varphi_2, k_1)}{K(k_1)} \qquad \text{for } -\infty < t < 0 \tag{16}$$

where the total electric flux terminating on the lower ground plane is

$$\int_{z=-ih}^{z=\infty-\imath h} \epsilon_0 \epsilon_r E_y dx = A_2 \frac{F\left(\arcsin\left[\tanh\left(\frac{\pi b}{2h}\right)\right], k_1\right)}{K(k_1)} \tag{17}$$

This expression yields an important result, since the measure of flux terminating on the lower ground plane determines the degree to which the coplanar-microstrip mode (CPM) occurs within grounded CPW's. Fig. 4(b) shows the cumulative distribution of electric flux across the lower ground plane as a function of the CPW's geometry.

The graphical plots calculated from (17) are shown in Fig. 5, which demonstrates the total electric flux terminating on the lower ground plane, with k and h/b as parameters.

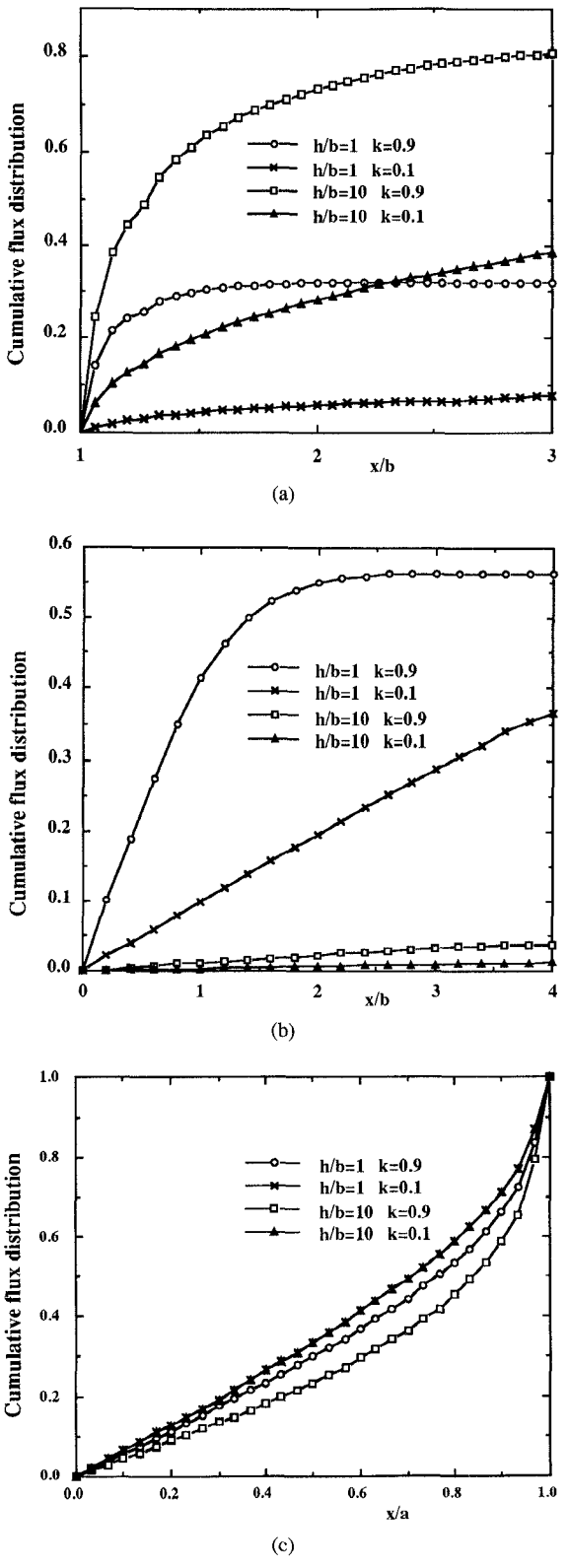

Fig. 4. Cumulative flux distribution as a function of the CPW's geometry, calculated as a fraction of A_2, (a) beneath the upper ground plane, (b) above the lower ground plane, and (c) beneath the center conductor.

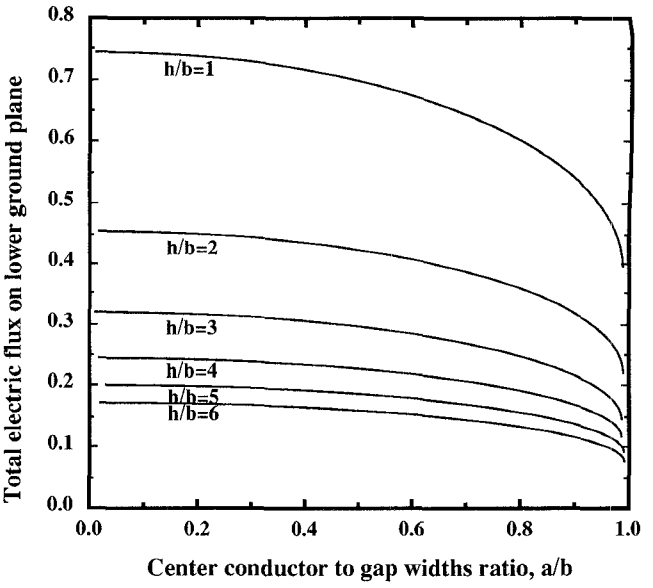

Fig. 5. Total electric flux terminating on the lower ground plane as a fraction of A_2, for variations in the CPW's geometry.

For constant A_2, the total flux terminating on the lower ground plane increases with increasing gap width and also with decreasing substrate thickness. From both Fig. 4(b) and Fig. 5, it is observed that while the cumulative distribution profiles increase in magnitude with increasing a/b, the actual total electric flux decreases as a/b increases. This behavior is explained by the fact that relatively wide center conductors, (as k approaches unity), cause the electric flux to be more confined directly underneath the center conductor, in contrast to a relatively narrow conductor, where the flux tends to spread widely across the ground conductors. As the substrate thickness h decreases for a fixed slot width, the characteristic behavior approaches that of a microstrip line, since a parallel plate mode also exists which has a reduced phase velocity relative to that of a CPW mode. This results in an increase in CPM mode of propagation which degrades the CPW transmission and return loss characteristics.

C. Center Conductor

The integral of the electric flux distribution over the center conductor surface within the substrate is

$$\int_{z=0+i0}^{z=x+i0} \epsilon_0 \epsilon_r E_y dx \propto \int_1^t \frac{dt}{\sqrt{t(t-t_3)(t-t_2)(t-1)}} = gF(\varphi_3, k_1) \qquad \text{for } 1 < t \leq t_2 \tag{18}$$

$$\varphi_3 = \arcsin \sqrt{\frac{t_2(t-1)}{t(t_2-1)}} = \arcsin \left[\coth\left(\frac{\pi a}{2h}\right) \tanh\left(\frac{\pi x}{2h}\right) \right] \tag{19}$$

Therefore

$$\int_{z=0+i0}^{z=x+i0} \epsilon_0 \epsilon_r E_y dx = A_2 \frac{F(\varphi_3, k_1)}{K(k_1)} \qquad \text{for } 1 < t \leq t_2 \tag{20}$$

where the total electric flux emanating from the center conductor into the substrate is given by:

$$\int_{z=0+i0}^{z=a+i0} \epsilon_0 \epsilon_r E_y dx = A_2 \frac{F(\varphi_3, k_1)}{K(k_1)}\bigg|_{\varphi_3=90^\circ} = A_2 \tag{21}$$

as expected. The variation in the cumulative flux distribution beneath the center conductor is plotted in Fig. 4(c), as h/b

and k vary. From this graph, it can be seen that 50% of the flux emanating from the center conductor into the substrate does so within the outermost 15% of the center conductor, for $h/b = 10$ and $k = 0.9$. This example is an extreme case where the effect of low impedance lines, (when k approaches unity), produces high E-field crowding at the center conductor edges, as predicted. It is noted that the cumulative electric flux distributions beneath the center conductor for high impedance lines ($a \ll b$) are hardly distinguishable from each other for varying substrate thicknesses, as shown in Fig. 4(c).

IV. Discussion

The rate of decay of electric field strength across the upper ground conductor indicates the coupling effects that would exist between adjacent CPW transmission lines. One result of this observation is that coupling between parallel CPW lines will decrease with decreasing substrate height, since the placing of the lower ground plane causes the electric flux to become more confined beneath the center conductor strip. At any rate, the presented graphs lend themselves to the design of compact MMIC's where the measure of adjacent line coupling of CPW's can be controlled. Narrow center conductors result in large insertion losses, as expected, and where the gap width $b - a$ increases the losses decrease, since the level of field crowding at the conductor edges decrease with k decreasing. With the center conductor width kept constant, insertion loss is reduced when the characteristic impedance of the line is increased. This may be thought of as a reduction in conductor loss with increased impedance due to the lower current flowing on the transmission line. Another expected outcome is that no edge singularities occur with regard to the lower ground plane, as expressed in (7b), resulting in no normal E-field crowding throughout this lower ground plane.

V. Conclusion

A new direct method of analyzing the normal electric field distribution for grounded CPW's has been proposed. The graphical results presented agree with previous analytical methods where the electric field distribution plots vary with CPW's structural dimensions, as predicted. While we have limited ourselves to the case of grounded CPW's where the substrate is of finite thickness, the method shown here may be employed to analyze CPW's with infinitely thick substrates, upper shielding, or without any lower ground plane. This method may also be applied to the CPW's normal magnetic field Hy across the surface of gap b-a.

We have described how a sequence of conformal mappings, in terms of complete and incomplete elliptic integrals, may be used to compute the cumulative electric flux distribution for the CPW's conductor surfaces. These mappings overcome singularities at the conductor edges, since the normal fields in the image domain are smooth everywhere. While successive transformations yield exact solutions, the presented equations for substrate thicknesses becoming comparable to the slot width become questionable, but they do lead to excellent results for most practical structures. The proposed method does not require successive iterative processing in order to compute the electric field distribution and, consequently, has the advantage of being particularly appropriate for design analysis of CPW's structures. Thus, the potential for application of the above techniques is well suited to computer aided design analysis with relatively little programming effort.

Acknowledgment

The authors would like to express their appreciation to Dr. A. H. Aghvami for his constant help and encouragement, and S. Lucyszyn for his constructive criticisms.

References

[1] K. C. Gupta, R. Garg, and I. J. Bahl, *Microstrip Lines and Slotlines*. Norwood, MA: Artech House, 1979.
[2] C. P. Wen, "Coplanar waveguide: A surface strip transmission line suitable for nonreciprocal gyromagnetic device applications," *IEEE Trans. Microwave Theory Tech.*, vol. MTT-17, pp. 1087–1090, Dec. 1969.
[3] C. P. Wen, "Coplanar waveguide directional couplers," *IEEE Trans. Microwave Theory Tech.*, vol. MTT-18, pp. 318–322, June, 1970.
[4] G. Ghione and C. Naldi, "Parameters of coplanar waveguides with lower ground planes," *Electron. Lett.*, vol. 19, no. 18, pp. 734–735, Sept. 1983.
[5] G. Ghione and C. Naldi, "Analytical formulas for coplanar lines in hybrid and monolithic MIC's," *Electron. Lett.*, vol. 20, no. 4, pp. 179–181, Feb. 1984.
[6] G. Ghione and C. Naldi, "Coplanar waveguides for MMIC applications: Effect of upper shielding, conductor backing, finite-extent ground planes, and line-to-line coupling," *IEEE Trans. Microwave Theory Tech.*, vol. MTT-35, pp. 260–267, Mar. 1987.
[7] T. Hatsuda, "Computation of coplanar-type strip-line characteristics by relaxation method and its application to microwave circuits," *IEEE Trans. Microwave Theory Tech.*, vol. MTT-23, pp. 795–802, Oct. 1975.
[8] S. S. Bedair, and I. Wolff, "Fast and accurate analytic Formulas for calculating the parameters of a general broadside-coupled coplanar waveguide for (M)MIC applications," *IEEE Trans. Microwave Theory Tech.*, vol. 37, pp. 843–850, May 1989.
[9] G. C. Liang, Y. W. Liu, and K. K. Mei, "Full-wave analysis of coplanar waveguide and slotline using the time-domain finite-difference method," *IEEE Trans. Microwave Theory Tech.*, vol. 37, pp. 1949–1957, Dec. 1989.
[10] D. Marcuse, "Electrostatic field of coplanar lines computed with the point matching method," *IEEE J. Quantum Electron.*, vol. 25, pp. 939–947, 1989.
[11] C. N. Chang, Y. C. Wong, and C. H. Chen, "Full-wave analysis of coplanar waveguides by variational conformal mapping technique," *IEEE Trans. Microwave Theory Tech.*, vol. MTT-38, pp. 1339–1344, Sept. 1990.
[12] Y. C. Shih, and T. Itoh, "Analysis of conductor-backed coplanar waveguide," *Electron. Lett.*, vol. 18, no. 12, pp. 538–540, June 1982.

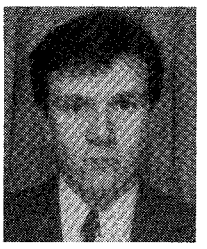

Matthew Gillick (S'92) was born in the Republic of Ireland, on June 16, 1966. He received the B.Eng. degree in electrical and electronic engineering (with first class honors) from King's College, University of London, in July 1990. He is currently working toward the Ph.D. degree in microwave engineering at the same University. His main research interests include the analysis and design of high power amplifiers, electromagnetic field theory, and the modeling of monolithic microwave integrated circuits (MMIC's) especially in coplanar waveguide structures.

Mr. Gillick received the Layton Scientific Research Award, and the Peplow Prize for academic achievement in 1990. Mr. Gillick currently holds a UK science and engineering research council CASE Award, in co-operation with British Aerospace Space Systems. He is a student Member of the Institution of Electrical Engineers, London.

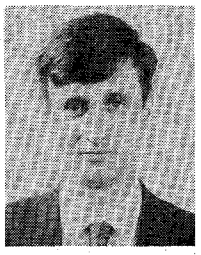

Ian D. Robertson (M'91) was born in London, England in 1963. He received his B.Sc. and Ph.D. degrees from King's College, University of London in 1984 and 1990, respectively. He was awarded the Siemens Prize, the IEE Prize, and the Engineering Society Centenary Prize for academic achievement in his final year.

From 1984 to 1986 he was employed at Plessey Research (Caswell) in the GaAs MMIC Research Group, where he worked on MMIC mixers, RF-on-wafer measurement techniques, and FET characterization. From 1986 to 1990 he was employed as a Research Assistant at King's College, and worked on satellite payload engineering and MMIC design. He is currently a Lecturer at King's, and leads the MMIC Research team in the Communications Research Group.

Jai S. Joshi (SM'91) received the Bachelor of Technology (Hons.) degree in electrial engineering in 1968 and the Master of Technology degree in electrical communication engineering in 1970, both from the Indian Institute of Technology, Bombay, India. In Sept. 1976, he successfully completed a part-time industry sponsored Ph.D., program on the analysis of waveguide post configurations with the Council for National Academic Awards (CNAA) London, England.

From 1970 to 1977, he worked at Mullard (Hazel Grove) Ltd as a microwave engineer working on research and development of transferred electron device oscillators. From 1977 to 1985 he worked at Allen Clark Research Center, Plessey Research (Caswell) Ltd as a Senior Principal Research Scientist. He was responsible for GaAs FET oscillators, power amplifiers and high frequency applications. He realized the world's first GaAs MMIC oscillator-on-a-chip in 1979. Since 1985 he has been Head of Communications Electronics in the Payload Engineering Department at British Aerospace (Space Systems). In this capacity, he leads a group of engineers in the research, design and development of on-board and ground segment payload equipments like LNA, solid state power amplifiers, GaAs MMIC's, control components, BFN's, etc.

Dr. Joshi has published several papers in leading international technical journals. He presently serves on the Editorial Board of the IEEE TRANSACTIONS on MICROWAVE THEORY AND TECHNIQUES. He is a Chartered Engineer and a Member of the Institution of Electrical Engineers, London.